Effect of cellular structure on the optical properties of wood

Mayuka Ban*, Tetsuya Inagaki*, Te Ma, and Satoru Tsuchikawa

Graduate School of Bioagricultural Sciences, Nagoya University, Furo-cho, Chikusa-ku, Nagoya 464-8601, Japan. E-mail: st3842@agr.nagoya-u.ac.jp

*Equally contributed to this manuscript (co-first author).

To construct robust calibrations of wood properties by near-infrared spectroscopy, one must independently evaluate the spectral contributions of light absorption and light scattering. However, the light propagation in wooded cellular structures is difficult to interpret because these structures are complex, heterogeneous, and anisotropic. This study investigates the reduced scattering coefficients of softwood and hardwood (with ring-porous or diffuse-porous vessels) at 846 nm by time-resolved spectroscopy. It also evaluates the effect of wooden cellular structure and dry air density on the light propagation. After determining the reduced scattering coefficients, we observed cross-sectional microscopic images of the wood samples. Eighty-five percent of the variation in the reduced scattering coefficients was explainable by the air-dry density, area ratio of the cell wall, and the median pore area. Monte Carlo simulations of the light propagation through wood revealed that most of the photon transport occurs in the cell-wall substance.

Keywords

Time resolved NIR spectroscopy, Multiple scattering, Turbid media, Wood, Monte-Carlo simulation

INTRODUCTION

The properties of wood (e.g., density, moisture content, grain angle, crystallinity and micro fibril angle) vary considerably between species and even among members of the same species. For quality assurance in industrial processes, nondestructive monitoring and control of the physical, mechanical, and chemical properties of wood are strongly desired. Near infrared (NIR) reflectance spectroscopy, which is mainly used in chemical composition analysis, is also an increasingly popular tool for monitoring the properties of wood. In many studies, the chemical, physical and mechanical properties of wood have been predicted by NIR reflectance spectroscopy aided by statistical methods (i.e., chemometrics).[1-3] However, such chemometric NIR approaches have several disadvantages. First, they cannot separate the spectral contributions of the light absorption and light scattering phenomena. Second, the construction of a calibration model requires a considerable amount of data, which is usually not transferable among instruments. Additionally, owing to its complex cellular structure, wood makes a significant light scattering contribution to the NIR spectra. Softwood possesses a mainly tracheid structure, arrayed along the longitudinal direction, whereas hardwood structures vary (e.g., tracheids, vessels, libriform wood fibers, or ray cells). The water retained in cell walls or cell lumens also significantly affects the optical properties of wood.[4] To construct a robust calibration of wood properties by NIR spectroscopy, we must independently evaluate the spectral contributions of light absorption (which results from harmonics or overtones of the fundamental absorptions of the molecular vibrations of cellulose, hemicellulose, lignin, extractives and water) and light scattering (caused mainly by the cellular structure).

Many studies have investigated light absorption and scattering in tissues such as human skin, fruit, leaves, and wood. Typically, light scattering is described by a scattering coefficient μ_s and a

reduced scattering coefficient μ'_s, which strongly depend on the physical structure of the tissue. μ'_s is defined as

$$\mu_s' = (1-g)\mu_s. \qquad (1)$$

where g is the mean cosine of the scattering angle. The optical absorption is a linearly increasing function of concentration of the chemical components, whose slope defines the absorption coefficient μ_a. D'Andrea et al. determined μ_a and μ'_s in the wavelength range 700–1040 nm for two kinds of wood species treated in different ways (dry, wet and degraded) by time-resolved reflectance spectroscopy with two different orientations of the optical fiber.[5] They obtained many interesting results. In all cases, the reduced scattering coefficient (μ'_s = 10-100 cm^{-1}) was much larger than the absorption coefficient (μ_a = 0.05-1.00 cm^{-1}), although the scattering spectra were constant over the corresponding wavelength ranges. Moreover, μ'_s strongly depended on the wood species (silver fir or sweet chestnut wood). The μ'_s was much smaller in wet wood than in dried wood because the refractive index was closer between the wood cell-wall substance and the water in the pores. D'Andrea et al. also evaluated the moisture content (MC) of wood through the absorption coefficient, and found a strong relationship between MC and the absorption coefficient at a specific wavelength.[6] We measured the optical properties of drying wood with MCs ranging from 10% to 200% using time-resolved NIR spectroscopy.[4] After independently determining μ'_s and μ_a, we found that dry pores dominated the scattering phenomenon. Therefore, we determined the drying processes of large and small pores during the periods of constant and decreasing drying rate, respectively. To identify the origin of scattering in wood, Kienle et al. compared the experimentally measured and Monte Carlo-simulated light propagations on the microstructure of silver fir.[7] Solving Maxwell's equations, they determined the tracheid-contributed μ'_s of wet and dry wood as 1.79 mm^{-1} and 6.68 mm^{-1} respectively. They also calculated the scattering coefficient

$\mu_{s\text{-}iso}$ sourced from scattering media other than tracheids (pits, ray cells, and rough borders between the lumen and wood cell-wall substance) by fitting the measured and simulated light propagations. Previously, we measured the true μ'_s and μ_a of the cell-wall substance in douglas fir using time-resolved NIR spectroscopy.[8] In that study, the samples were saturated with hexane, toluene or quinolone to minimize the multiple light reflections on the boundary between the pores and cell-wall substance in the wood. μ'_s was minimized when the wood was saturated with toluene, which has a similar refractive index to the wood cell-wall substance. The optical parameters of the wood cell-wall substance were calculated as μ_a = 0.030 mm^{-1} and μ'_s = 18.4 mm^{-1}.

The cellular structures of wood are complex, heterogeneous, and anisotropic. Therefore, the cellular structure (which causes multiple light reflections) significantly differs between wood species; accordingly, the scattering coefficients highly depend on the wood species. Hardwood species especially have various cell arrangements, i.e., ring-porous, diffuse-porous, radial-porous, and figured-porous. Although the optical parameters of wood have been well clarified, the effect of cellular structure on μ'_s has not been fully investigated. Hans et al. investigated the relation between the μ_a and μ'_s values and the air-dry density of softwood and hardwood. They reported a weak relation between μ'_s and the air-dry density of wood, which was explained by the anatomical differences between the wood species.

In this study, we evaluate the softwood and hardwood (with ring-porous or diffuse-porous vessels) and evaluate the effects of wood structure and air-dry density on the light scattering. From cross-sectional microscopic images of the wood samples, we then determine the maximum pore diameter, the number of observed pores, the median and average pore areas, and the area ratio of the cell wall, and investigate their effects on μ'_s.

MATERIAL AND METHOD

Samples

Thirteen species of air-dried wood samples - five softwood species (*Agathis alba* Foxw, *Araucaria heterophylla, Thuja plicata, Chamaecyparis obtusa, Cryptomeria japonica*) and eight hardwood species (*Triplochiton scleroxylon, Hevea brasiliensis, Liriodendron tulipifera, Cercidiphyllum japonicum, Paulownia tomentosa, Kalopanax pictus, Fraxinus mandshurica, Fagus sylvatica*) - were selected for the study (see Table 1). The sample dimensions were 2 mm thick (tangential or radial) × 80 mm (tangential or radial) × 150 mm (longitudinal). We prepared 3 samples for each species.

Time-resolved NIR spectroscopic measurements

Time-resolved NIR spectroscopic measurements were performed with a picosecond pulsed laser with a wavelength of 846 nm, a pulse width of 70 ps, and a beam diameter on the sample of approximately 1.5 mm (PLP-10, Hamamatsu Photonics Co., Hamamatsu, Japan). The transmitted photons were dispersed with a spectroscope equipped with gratings (C11119-02, A13302-02, Hamamatsu Photonics Co., Hamamatsu, Japan). To detect time-resolved data, the time variation of the transmitted radiation intensity was recorded by a streak camera with a time resolution of 10.3 ps (C5680, Hamamatsu Photonics Co., Hamamatsu, Japan). The combination of NIR spectroscopy and streak camera (which directs the incoming photons onto a photocathode that emits electrons via the photoelectric effect) is also called time-of-flight (TOF) NIR spectroscopy. The wood sample was placed 90 mm from the pulsed laser, and the transmitted photons exiting the sample were collected by a 300 μm-diameter optical fiber (length: 3 m, A5760-02, Hamamatsu Photonics Co., Hamamatsu, Japan) placed 2 mm from the sample, and passed to the spectrometer. The instrument response function (IRF) was measured with a neutral density filter with a 1% transmission ratio (A5760-02, Hamamatsu Photonics Co., Hamamatsu, Japan) placed directly in

front of the camera slit. The time-resolved profiles (TRPs) were acquired at the opposite side of the incident beam on the radial-longitudinal section with a time range of 1 ns, and measured 3 times at different points. Each photon count was performed for 60 s. As we anticipated the position of incident light on wood has significant effect on the light propagation and μ'_s, we used relatively big beam diameter (approximately 1.5 mm) and repeat the measure on three different point and averaged for each samples.

TRP analysis

The measured TRP can be expressed as a convolution between the IRF and true photons in the time-resolved distribution (TRD) as equation (2):

$$\mathrm{TRP} = \mathrm{IRF} \times \mathrm{TRD}. \quad (2)$$

where × denotes the convolution operator. The absorption (μ_a : mm^{-1}) and reduced scattering coefficient (μ'_s: mm^{-1}) were computed by fitting the convolution between the IRF and the model TRD to the measured TRP. The model TRD was obtained by solving the diffusion approximation equation for an infinite slab with extrapolated transmittance boundary conditions.[9] When calculating the refraction indices n_{wood} of the wood samples, we assumed $n_{cw} = 1.55$ and $n_{air} = 1.00$ as the refraction indices of the wood cell walls and air, respectively.[8] The TRP was analyzed in Matlab R2015b (MathWorks, Inc., MA, USA), and the sum of the differences between the theoretical and measured TRPs was minimized by a fitting procedure implemented by the interior point algorithm.

Microscopic observations

To investigate the relation between μ'_s and the wood texture, we observed cross-sectional microscopic images of the wood samples after measuring their TRPs. Each wood sample was cut into 3 equally sized pieces, each including one incident point (giving a total of 39 small pieces).

The densities of the small pieces were calculated as the weight divided by the volume. The pieces were sliced by a microtome, then dyed with safranin solution for cross-sectional microscopic imaging (2560×1920 pixels corresponding to 1.12×0.84 mm) under a bright-field microscope (PrimoStar, Carl Zeiss Microscopy Co., Japan). We acquired 10 cross-sectional images at different positions on each piece. After binarizing the images, pores were identified as connected components more than 10 pixels across. We calculated the diameter of the maximum pore (μm), the number of determined pores, the median, and average pore area (μm^2), and the cell-wall area ratio in each image, and averaged them over 30 images. The binarization and parameter calculations were performed in Matlab R2015b.

Monte Carlo simulations of light propagation in wood

To understand light propagation through the wood, we simulated the absorption distribution of the light propagation in a three-dimensional (3D) wood structure model. The simulations were performed in the Monte Carlo code, MCVM (Monte Carlo modeling of photon migration in Voxelized Media), which has been verified against the gold standard MCML (Monte Carlo modeling of light transport in Multi-Layered tissue),[10] and which effectively simulates light photon migration in a 3D heterogeneity model. The MCVM algorithm is detailed in the literature.[11] As wood is a natural product with a complex structure, the reflective indices of the cell wall (n_{cw} = 1.55) and air (n_{air} = 1.00) are widely different, causing specular reflections and transmissions. The refractive-index mismatch at the boundaries are also considered to improve the precision of simulations in MCVM code. Figure 1 shows the steps of the MCVM simulations. First, the cross-sectional microphotograph of each wood sample was changed to a binary image through thresholding image processing. The resulting 2D binary image was copied to make a 3D structure model. The dimensions of the generated 3D wood structure model were (256×256×114) voxels,

158 with pixel intervals corresponding to 4.4 μm. The tissue type was described by its optical
159 properties: the reflective index n, μ_s, μ_a and, g. Adjacent voxels with the same optical properties
160 were assigned to the same type of tissue. In this study, the 3D model comprised two tissue types
161 (wood cell-wall and air). As the true optical parameters (at 846 nm) of the wood cell walls, we
162 adopted the values calculated by Kitamura et al.[9] In the air parts, we assumed $\mu_a = 0$ mm^{-1}, $\mu_s = 0$
163 mm^{-1}, and $n = 1$. The total number of incident photons was 10^6 and the vertical incident point
164 (although the actual light source diameter was 1.5 mm which is not regarded as the point light)
165 was the surface center of the 3D model. To obtain the time-resolved information, we set the time
166 interval to 1 ps and acquired 5 snapshots from 1 ps to 5 ps. Tissue modeling and image processing
167 were performed in Matlab2013a (The Mathworks Inc., Natick, MA, USA).

168 **RESULT AND DISCUSSION**

169 **Relation between air-dry density and reduced scattering coefficient**

170 Figure 2 shows the TRP of air-dry agathis wood (air-dry density $\rho_{\text{airdry}} = 0.33$ g/cm^3), and the $\mu's$
171 values computed by fitting the TRP to the IRF convoluted with TRD. Figure 3 shows the relation
172 between the air-dry density and the acquired $\mu's$ values of the softwood, ring-porous wood, and
173 diffuse-porous wood. There is a significant positive relation between air-dry density and $\mu's$
174 (determination coefficient $R^2 = 0.59$). The R^2 of softwood, diffuse-porous vessels and ring-porous
175 vessels were 0.55, 0.49, and 0.73, respectively. The acquired $\mu's$ of air-dry wood ranged from 8.9
176 to 30.9 mm^{-1}, although Hans et al.[12] reported $\mu's = 15.3 \pm 0.3$ mm^{-1} and $\mu's = 17.4 \pm 0.9$ mm^{-1}
177 respectively for air-dry hinoki cypress (*Chamaecyparis obtusa*) and Japanese larch (*Larix*
178 *kaempferi*) at 846 nm, and D' Andrea et al.[5] reported $\mu's \approx 10$ mm^{-1} for air-dry silver fir at 840 nm.
179 The light scattering in wood is complex and caused by multiple factors: (1) the interaction of light
180 with small particles with different refractive indices from the surrounding materials, (2) a

refractive-index mismatch between the cell-wall substance and lumens in the wood, (3) scattering at the rough border between the lumen of the tracheid and the wood cell-wall substance, and (4) scattering due to the birefringent nature of the cellulose microfibril or the spatial distribution of chemical components in the wood cell-wall substances. As the types of cells (tracheids, ray cells, vessels), shapes of cells (among cell types and between earlywood and latewood), and vessel alignments (ring-porous, diffuse-porous, radial-porous, and figured-porous) differ widely among wood species, the scattering coefficients should also differ among the wood species. The significant positive relation between air-dry density and μ'_s can be explained by the increased volume fraction of the wood cell-wall substance (which scatters the NIR light) as the wood density increases. The measured μ'_s of ayous (*Triplochiton scleroxylon*) and rubber tree (*Hevea brasiliensis*: with diffuse-porous vessel structures) are much higher than estimated from the regression line, with air-dry densities of 0.44 g/cm^3 and 0.70 g/cm^3, respectively. The higher scattering in these wood species is attributed mainly to light scattering between the lumen and the wood cell-wall substance for all cell types, which results from the index-mismatching effect. To investigate the relation between μ'_s and the cell-shape parameters, namely, the maximum pore diameter (μm), number of observed pores, median and mean pore areas (μm^2) and the cell-wall area ratio, we computed the cell-shape parameters from the cross-sectional microscopic images.

Relations between parameters calculated from microscopic image and reduced scattering coefficient

Figure 4 shows representative microscopic images of (a) softwood (western red cedar: *Thuja plicata*), (b) diffuse-porous vessel hardwood (beech: *Fagus sylvatica*) and (c) ring-porous vessel hardwood (castor aralia: *Kalopanax pictus*). Their corresponding binary images are shown in panels (d)–(f). The density, μ'_s and texture parameters calculated from the microscopic images

were averaged over the three samples and are summarized in Table 1. Correlation coefficient between cellular structure parameters calculated from microscopic cross-sectional images of the wood samples were summarized in Table 2. The correlation coefficient value between ρ_{airdry} and area ratio of cell wall, which had been expected to be close to one, was not high as expected (0.77), because only the connected components more than 10 pixels across was recognized as pores.

Among the five calculated parameters, the cell-wall area ratio and median pore area were significantly related to μ'_s (see Figure 5). When all samples were included in the calculation, μ'_s was a quadratic function of the cell-wall area ratio (R^2 = 0.76), and an exponential function of the median pore area (R^2 = 0.54). We calculated the R^2 values between measured μ'_s and estimated value from the exponential, linear, logarithmic, quadratic regression for each five calculated parameters and decide the best relation (quadratic function for the cell-wall area ratio and exponential function for the median pore area) giving the highest R^2. However, μ'_s was weakly linearly correlated with both parameters in softwood (R^2 = 0.044 and 0.110 for area ratio and median pore area respectively; see Figure 5 (c) and (d)), but significantly linearly correlated with both parameters in the diffuse-porous and ring-porous hardwoods. In hardwood, the positive relation between μ'_s and the area cell-wall ratio can be explained by the high volume fraction of the wood cell-wall substance, which scatters the NIR energy. Meanwhile, as the median pore area increases, the light is less likely to penetrate the boundary between the cell wall and air, so the decreases. However, as softwoods are also much simpler with more periodic anatomical features than hardwoods, the effect of both parameters on μ'_s was small.

Considering the relationships in Figure 5, we estimated μ'_s from the density, cell-wall area ratio, and median pore area of the wood samples. The equation is given by

$$\mu_s^{'} = \mathrm{a} \times \rho_{\mathrm{airdry}} + \mathrm{b} \times r^2 + \mathrm{c} \times r + \mathrm{d} \times S^{\mathrm{e}} + \mathrm{f}. \qquad (3)$$

where r and S denote the area ratio of the cell wall and the median pore area, respectively, and the coefficients a, b, c, d, e and f were determined by a nonlinear curve-fitting method, (i.e., the simplex method) that minimizes the residue between the measured μ'_s and those predicted by Eq. (3). Figure 6 (a) plots the relation between the measured μ'_s and those predicted by Eq. (4).

$$\mu_s' = 23.54 \times \rho_{\text{airdry}} + 196.79 \times r^2 - 232.33 \times r + 45.03 \times S^{68.01} + 69.90. \qquad (4)$$

where the coefficients minimize the residues between the measured and predicted values of all wood samples. These three parameters (density, cell-wall area ratio and median pore area) explain 85% of the variation in the μ'_s of wood ($R^2 = 0.85$).

We also constructed the regression curves of the separate woods (softwood, diffuse- porous hardwood and ring-porous hardwood) by Eq. (5):

$$\mu_s' = \mathrm{g} \times \rho_{\text{airdry}} + \mathrm{h} \times r + \mathrm{i} \times S + \mathrm{j} \qquad (5)$$

The R^2 values of softwood, diffuse-porous vessel hardwood and ring-porous vessel hardwood were 0.57, 0.93, and 0.83, respectively. The individual plots are shown in Figure 6(b).

Light propagation simulations by the Monte Carlo method

Figure 7 shows the simulated light propagation in japanese cedar (*Cryptomeria japonica)*, agathis (*Agathis alba* Foxw), empress tree (*Paulownia tomentosa*), yellow poplar (*Liriodendron tulipifera)*, and rubber wood. In the simulation the vertical incident point light was emitted on the wood surface although the actual light source diameter was 1.5 mm. However, we can roughly recognize the light propagation in the wood from the simulation. These five representative wood species cover a wide range of μ'_s, ρ_{airdry}, r and S. As absorption distribution were simulated in this figure, there are no photons on the pixel corresponding to air. The Monte Carlo code, MCVM simulated the light propagation in wood extremely well; in particular, the photons spread through a small area in woods with relatively small μ'_s, i.e., japanese cedar (Figure 7(a)) and agathis (Figure

7(b)), and through a wide area in woods with relatively large μ'_s, i.e., yellow poplar (Figure 7(d)) and rubber tree (Figure 7(e)). Note also that the photons spread further when the cell walls were continuously connected, as observed in yellow poplar and rubber tree (Figure 7(d) and (e)). Moreover, the photons spread around the pore, which explains the significant effect of the area cell-wall ratio r and median pore area S on μ'_s. As the cell wall thickens and the degree of continuous connectivity increases, the r enlarges and the S reduces, thereby increasing the μ'_s.

This study investigated the effect of air-dry density and wood texture properties on the reduced scattering coefficient μ'_s. We believe that the interpretation of scattering phenomenon in wood enable us to construct robust regression model for the estimation of moisture content or chemical concentration without using chemometrics approach such as PLSR. Three fiber based diffuse reflectance spectroscopy (TFDRS),[13] which is possible to construct the handheld device using LEDs as a light source, is one of the prominent method, because the a proposed parameter γ in this method, which is calculated using the ratio of light intensity detected at two difference distances from light source, is independent of the optical path length and exhibits good linear correlation with the analyte material concentration. The interpretation and determination of scattering properties in wood lead to the determination of the optimal optical system for TFDRS.

CONCLUSIONS

This study investigated the effect of air-dry density and wood texture properties on the reduced scattering coefficient μ'_s, measured by time-resolved spectroscopy at 846 nm. The wood texture parameters were calculated from cross-sectional microscopic images of the prepared wood samples. μ'_s was linearly related to the air-dry density (R^2 = 0.56), quadratically related to the cell-wall area ratio (R^2 = 0.76), and exponentially related to the median pore area (R^2 = 0.54). Eighty-five percent of the variation in the μ'_s of wood samples can be explained by these three parameters.

Next, the light propagation was simulated in the cross-sectional microscopic images. In these simulations, the photons spread further in woods with continuously connected cell walls. The significant effect of cell-wall area ratio and median pore area on μ'_s were attributable to the thicker, more connected cell walls associated with large cell-wall area ratio and small median pore area. Accordingly, increasing the area ratio of the cell wall and decreasing the pore area increased the μ'_s.

ACKNOWLEDGMENT

The authors would like to acknowledge the financial support from JSPS (KAKENHI, No. 16K07805 and No. 19380099).

REFERENCES

1. S. Tsuchikawa, "A review of recent near infrared research for wood and paper," *Appl. Spectrosc. Rev.* **42**, 43 (2007).

2. S. Tsuchikawa and M. Schwanninger, "A review of recent near-infrared research for wood and paper (part 2)", *Appl. Spectrosc. Rev.* **48**, 560 (2013).

3. S. Tsuchikawa and H. Kobori, "A review of recent application of near infrared spectroscopy to wood science and technology", *J. Wood Sci.* **61**, 213 (2015).

4. K. Konagaya, T. Inagaki, R. Kitamura and S. Tsuchikawa, "Optical properties of drying wood studied by time-resolved near-infrared spectroscopy", *Opt. Express* **24**, 9561 (2016).

5. C. D'Andrea, A. Farina, D. Comelli, A. Pifferi, P. Taroni, G. Valentini, R. Cubeddu, L. Zoia, M. Orlandi and A. Kienle, "Time-resolved optical spectroscopy of wood," *Appl. Spectrosc.* **62**, 569 (2008).

6. C. D'Andrea, A. Nevin, A. Farina, A. Bassi and R. Cubeddu, "Assessment of variations in moisture content of wood using time-resolved diffuse optical spectroscopy", *Appl. Optics* **48**, B87 (2009).

7. A. Kienle, C. D'Andrea, F. Foschum, P. Taroni and A. Pifferi, "Light propagation in dry and wet softwood", *Opt. Express* **16**, 9895 (2008).

8. R. Kitamura, T. Inagaki and S. Tsuchikawa, "Determination of true optical absorption and scattering coefficient of wooden cell wall substance by time-of-flight near infrared spectroscopy", *Opt. Express* **24**, 3999 (2016).

9. M. S. Patterson, B. Chance and B. C. Wilson, "Time resolved reflectance and transmittance for the noninvasive measurement of tissue optical-properties", *Appl. Optics* **28**, 2331 (1989).

10. L. Wang, S.L. Jacques and L. Zheng, "MCML-Monte Carlo modeling of light transport in multi-layered tissues", *Comput. Meth. Prog. Bio.* **47**, 131 (1995).

11. T. Li, H. Gong and Q. Luo, "MCVM: Monte Carlo Modeling of Photon Migration in Voxelized Media", *J. Innov. Opt. Health Sci.* **3**, 90 (2010).

12. G. Hans, R. Kitamura, T. Inagaki, B. Leblon and S. Tsuchikawa, "Assessment of variations in air-dry wood density using time-of-flight near-infrared spectroscopy", *Wood Mater. Sci. Eng.* **10**, 57 (2014).

13. T. Inagaki, D. Nozawa, Y. Shimomura and S. Tsuchikawa, "Three-fibre-based diffuse reflectance spectroscopy for estimation of total solid content in natural rubber latex", *J. Near Infrared Spec.* **24**, 327 (2016).

Figure captions

Figure 1. Modeling the photon migration in a voxelized 3D wood structure model.

Figure 2. Measured time-resolved profiles of 70-ps 846-nm pulses transmitted through air-dry wood samples. Black dots show the normalized numbers of photons transmitted through the wood sample, and the red solid curve is fitted by the diffusion model.

Figure 3. Relation between wood air-dry density and μ'_s. Filled square, open square, and open triangle are the data from softwood, ring-porous vessel hardwood and diffuse-porous vessel hardwood, respectively.

Figure 4. Microscopic images of (a) western red cedar (softwood), (b) beech (diffuse-porous vessel hardwood), and (c) castor aralia (ring-porous vessel hardwood). (d), (e) and (f) are the binary images of (a), (b) and (c), respectively.

Figure 5. Relations between μ'_s and (a) (c) area ratio of cell wall, and (b) (d) median pore area. The quadratic and exponential regression lines in (a) and (b) respectively describe the variation of μ'_s among all wood samples, while the linear regression lines in (c) and (d) were determined for each kind of wood. Filled square, open square, and open triangle denote softwood, ring-porous vessel hardwood and diffuse-porous vessel hardwood, respectively.

Figure 6. Relation between measured and μ'_s predicted by (a) Eq. (2) for all wood species and (b) predicted by Eq. (3) for each kind of wood. Filled square, open square, and open triangle denote softwood, ring-porous vessel hardwood and diffuse-porous vessel hardwood, respectively.

Figure 7. Light propagation in (a) japanese cedar (b) agathis (c) empress tree (d) yellow poplar and (e) rubber wood simulated by the Monte Carlo method.

Table 1. Air-dry densities, μ'_s values and cellular structure parameters calculated from microscopic cross-sectional images of the wood samples.

Table 2. Correlation between cellular structure parameters calculated from microscopic cross-sectional images of the wood samples.

Figure 1. Modeling the photon migration in a voxelized 3D wood structure model.

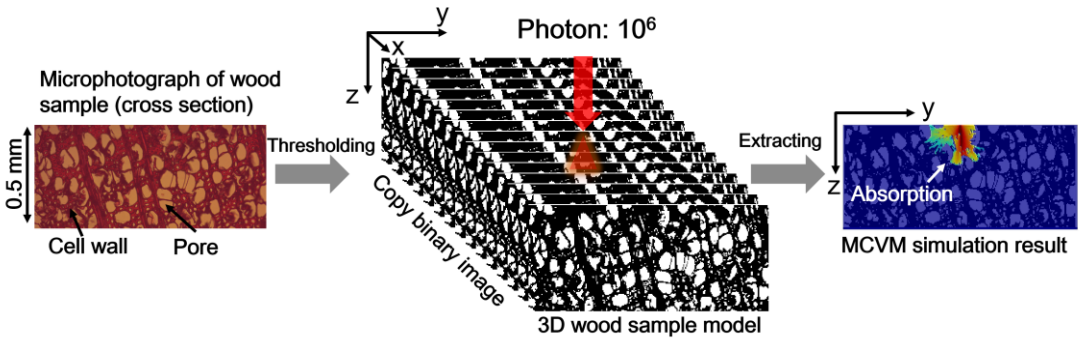

353

354 Title: Effect of cellular structure on the optical properties of wood

355 Authors: Mayuka Ban, Tetsuya Inagaki, Te Ma, and Satoru Tsuchikawa

356

357

358

359

360

361

362

363

364

Figure 2. Measured time-resolved profiles of 70-ps 846-nm pulses transmitted through air-dry wood samples. Black dots show the normalized numbers of photons transmitted through the wood sample, and the red solid curve is fitted by the diffusion model.

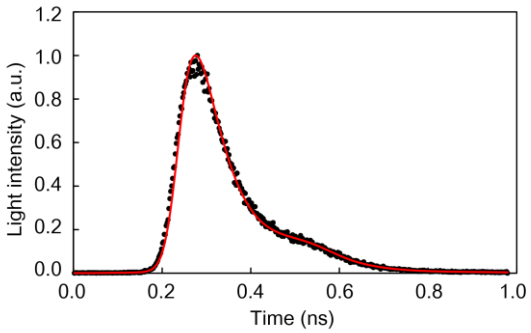

Title: Effect of cellular structure on the optical properties of wood

Authors: Mayuka Ban, Tetsuya Inagaki, Te Ma, and Satoru Tsuchikawa

Figure 3. Relation between wood air-dry density and μ'_s. Filled square, open square, and open triangle are the data from softwood, ring-porous vessel hardwood and diffuse-porous vessel hardwood, respectively.

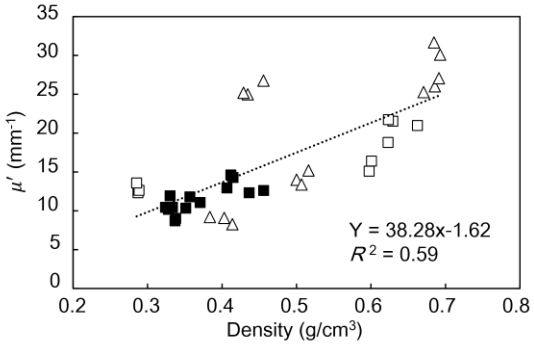

Title: Effect of cellular structure on the optical properties of wood

Authors: Mayuka Ban, Tetsuya Inagaki, Te Ma, and Satoru Tsuchikawa

Figure 4. Microscopic images of (a) western red cedar (softwood), (b) beech (diffuse-porous vessel hardwood), and (c) castor aralia (ring-porous vessel hardwood). (d), (e) and (f) are the binary images of (a), (b) and (c), respectively.

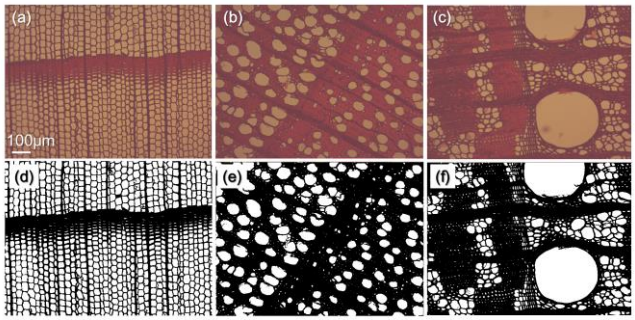

Title: Effect of cellular structure on the optical properties of wood

Authors: Mayuka Ban, Tetsuya Inagaki, Te Ma, and Satoru Tsuchikawa

Figure 5. Relations between $\mu's$ and (a) (c) area ratio of cell wall, and (b) (d) median pore area. The quadratic and exponential regression lines in (a) and (b) respectively describe the variation of $\mu's$ among all wood samples, while the linear regression lines in (c) and (d) were determined for each kind of wood. Filled square, open square, and open triangle denote softwood, ring-porous vessel hardwood and diffuse-porous vessel hardwood, respectively.

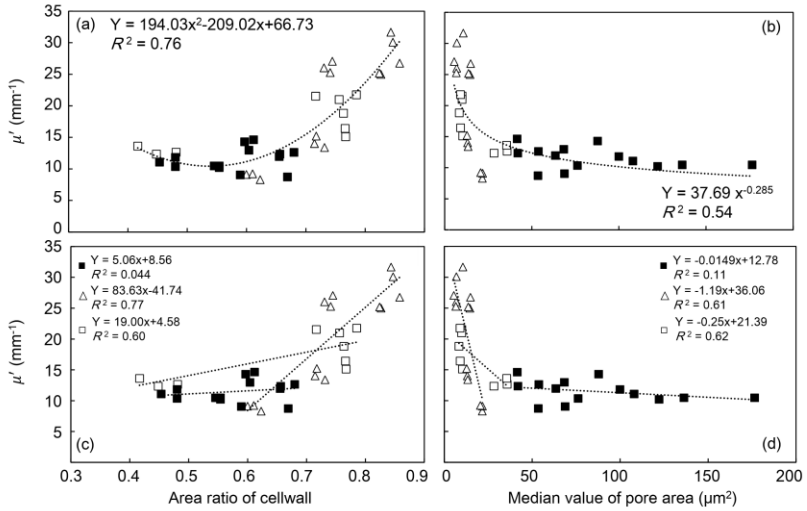

Title: Effect of cellular structure on the optical properties of wood

Authors: Mayuka Ban, Tetsuya Inagaki, Te Ma, and Satoru Tsuchikawa

Figure 6. Relation between measured and μ'_s predicted by (a) Eq. (2) for all wood species and (b) predicted by Eq. (3) for each kind of wood. Filled square, open square, and open triangle denote softwood, ring-porous vessel hardwood and diffuse-porous vessel hardwood, respectively.

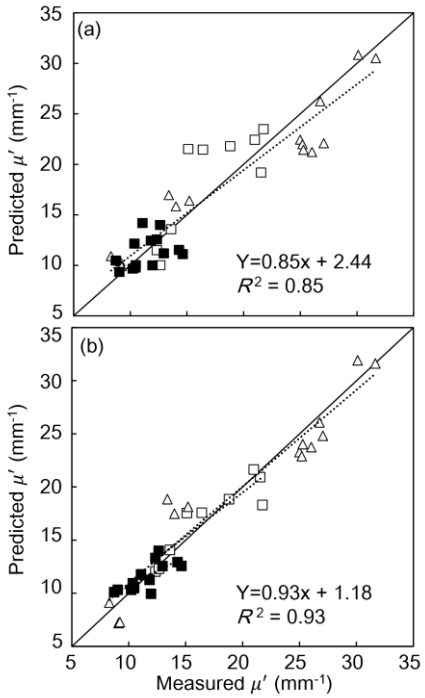

Title: Effect of cellular structure on the optical properties of wood

Authors: Mayuka Ban, Tetsuya Inagaki, Te Ma, and Satoru Tsuchikawa

Figure 7. Light propagation in (a) japanese cedar (b) agathis (c) empress tree (d) yellow poplar and (e) rubber wood simulated by the Monte Carlo method.

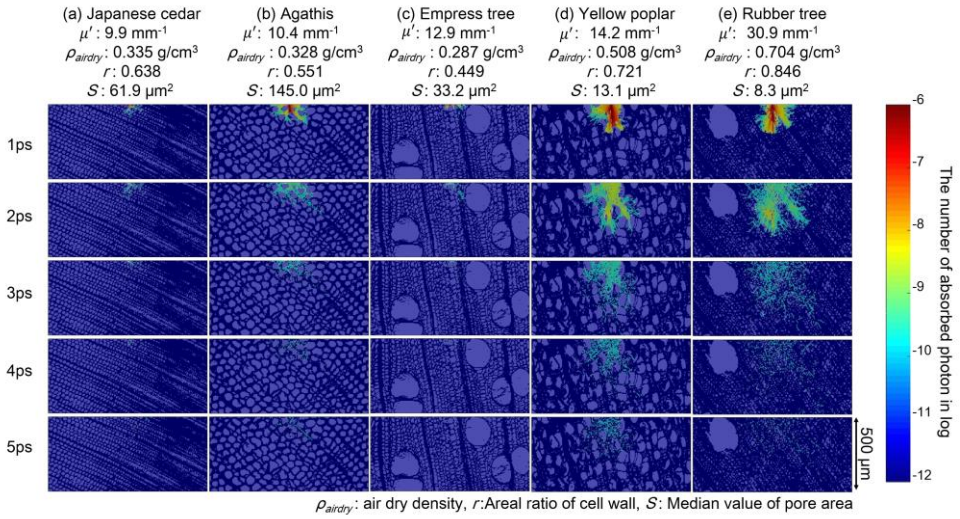

Title: Effect of cellular structure on the optical properties of wood

Authors: Mayuka Ban, Tetsuya Inagaki, Te Ma, and Satoru Tsuchikawa

442 **Table 1.** Air-dry densities, $\mu's$ values and cellular structure parameters calculated from

443 microscopic cross-sectional images of the wood samples.

Wood type	Name	Density (g/cm^3)	$\mu's$ (mm^{-1})	Regarded pore	Max. diameter (μm)	Mean pore rea (μm^2)	Median pore area (μm^2)	Cellwall area ratio
Softwood (No vessel)	Agathis	0.33±0.00	10.38±0.15	469±74	24.75±1.30	161.67±26.77	145.00±28.17	0.55±0.00
	Norfork island pine	0.41±0.00	13.96±0.88	883±147	17.30±0.70	76.12±13.33	65.89±23.20	0.60±0.01
	Western red cedar	0.36±0.01	11.09±0.73	894±78	19.60±0.85	98.35±11.49	94.71±16.56	0.47±0.02
	Hinoki cypress	0.45±0.01	12.49±0.20	1113±126	13.04±0.65	50.16±3.91	48.55±6.06	0.66±0.01
	Japanese cedar	0.33±0.00	9.90±1.78	931±52	14.52±0.26	63.93±5.98	61.93±7.74	0.64±0.04
Hardwood (Diffuse-porous)	Ayous	0.44±0.01	25.65±0.97	769±77	76.39±5.00	33.85±0.60	14.37±0.64	0.84±0.02
	Rubber tree	0.70±0.03	30.88±1.10	1033±130	82.43±4.42	25.79±3.35	8.32±2.02	0.85±0.00
	Yellow poplar	0.51±0.01	14.21±0.92	598±45	33.20±0.39	71.95±9.54	13.08±0.31	0.72±0.01
	Katsura tree	0.40±0.02	8.88±0.50	820±23	30.40±1.29	75.70±2.78	21.33±0.63	0.61±0.01
	Beech	0.68±0.01	26.13±0.89	689±151	29.65±0.47	63.40±17.27	6.32±0.75	0.74±0.01
Hardwood (Ring-porous)	Empress tree	0.29±0.00	12.87±0.66	1368±152	82.27±2.30	70.93±7.66	33.19±4.27	0.45±0.03
	Castor aralia	0.61±0.01	16.78±1.88	842±30	73.11±4.29	50.07±1.05	9.26±1.01	0.77±0.00
	Ash	0.64±0.02	21.42±0.39	513±14	91.88±8.48	71.59±17.90	9.63±0.54	0.75±0.03

444 Title: Effect of cellular structure on the optical properties of wood

445 Authors: Mayuka Ban, Tetsuya Inagaki, Te Ma, and Satoru Tsuchikawa

446

447

448

449

450

451

452

453

454 **Table 2.** Correlation between cellular structure parameters calculated from microscopic cross-
455 sectional images of the wood samples.

	Density (g/cm^3)	Regarded pore	Max. diameter (μm)	Mean pore rea ($μm^2$)	Median pore area ($μm^2$)	Cellwall area ratio
Density	1.00					
Regarded pore	-0.31	1.00				
Max. diameter	0.39	0.11	1.00			
Mean pore rea	-0.46	-0.45	-0.40	1.00		
Median pore area	-0.64	-0.17	-0.54	0.83	1.00	
Cellwall area ratio	0.77	-0.33	0.39	-0.62	-0.64	1.00

456 Title: Effect of cellular structure on the optical properties of wood

457 Authors: Mayuka Ban, Tetsuya Inagaki, Te Ma, and Satoru Tsuchikawa

458